iScience

CellPress
OPEN ACCESS

Article

Improved sparrow search algorithm optimization deep extreme learning machine for lithium-ion battery state-of-health prediction

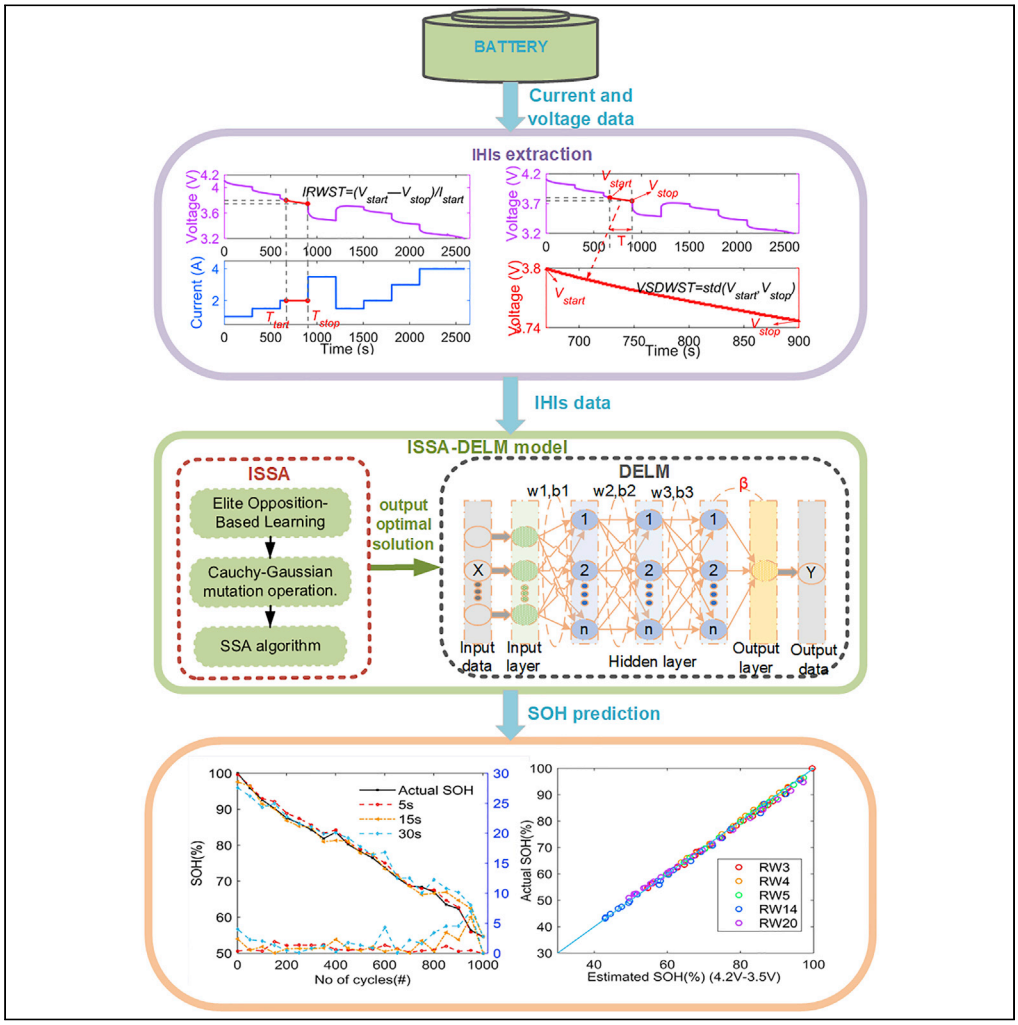

Jianfang Jia, Shufang Yuan, Yuanhao Shi, Jie Wen, Xiaoqiong Pang, Jianchao Zeng

jiajianfang@nuc.edu.cn

Highlights

An ISSA-DELM method is used to predict the battery state-of-health

Two indirect health indicators are extracted from the partial discharging data

EOBL and Cauchy-Gaussian mutation strategy are utilized to improve SSA

The proposed approach obtains better prediction accuracy in shorter computation time

Jia et al., iScience 25, 103988
April 15, 2022
https://doi.org/10.1016/j.isci.2022.103988

iScience

CellPress
OPEN ACCESS

Article

Improved sparrow search algorithm optimization deep extreme learning machine for lithium-ion battery state-of-health prediction

Jianfang Jia,[1,3,*] Shufang Yuan,[1] Yuanhao Shi,[1] Jie Wen,[1] Xiaoqiong Pang,[2] and Jianchao Zeng[2]

SUMMARY

Accurate state-of-health (SOH) prediction of lithium-ion batteries (LIBs) plays an important role in improving the performance and assuring the safe operation of the battery energy storage system (BESS). Deep extreme learning machine (DELM) optimized by the improved sparrow search algorithm (ISSA) is developed to predict the SOH of LIBs under random load conditions in the paper. Firstly, two indirect health indicators are extracted from the random partial discharging voltage and current data, which are chosen as the inputs of DELM by the Pearson correlation analysis. Then, ISSA is presented by combining the elite opposition-based learning (EOBL) and the Cauchy-Gaussian mutation strategy to increase the diversity of sparrow populations and prevent them from falling into the local optimization. Finally, the ISSA-DELM model is utilized to estimate the battery SOH. Experimental results illustrate the high accuracy and strong robustness of the proposed approach compared with other methods.

INTRODUCTION

Lithium-ion batteries (LIBs) are the core elements of Battery Energy Storage Systems (BESS) because they are characterized by high specific energy, high efficiency, low maintenance, and long life (Kim et al., 2019). The performance of batteries gradually deteriorates with the increase of service time, which might not only affect the normal operation of electrical equipment but also bring about serious accidents (Saha et al., 2009; Xie et al., 2020). The state of health (SOH) is a measure of the battery life and plays a vital role in improving the performance of BESS and realizing timely maintenance of equipment. SOH is expressed as the ratio of the current maximum allowable discharge capacity to the nominal capacity of a new battery:

$$SOH = \frac{C_t}{C_0} \times 100\% \quad \text{(Equation 1)}$$

where C_t and C_0 represent the available capacity at time t and the nominal capacity of a new battery, respectively. It is deemed to reach the end-of-life (EOL) when the capacity of the LIBs drops below 80% of the nominal capacity.

The SOH of LIBs relies on the materials used for battery design and two electrodes, but it is affected by operational conditions such as environmental temperature and discharge current (Panchal et al., 2018; Rosa Palacin, 2018, Jia et al., 2021a). Considering that the battery will be charged when it is not discharged to the cut-off voltage in actual operation, Yang et al. (Yang et al., 2021) used partial discharge voltage and temperature of LIBs to realize the online prediction of SOH. Pang et al. (Pang et al., 2019) proposed the combination of the wavelet decomposition technology (WDT) and the Nonlinear Auto-Regressive neural network (NARNN) model to capture the capacity regeneration phenomenon of LIBs. Jia et al. (Jia et al., 2021b) presented a combination of Wavelet neural network (WNN) with Unscented particle filter (UPF) model to predict the battery SOH. However, these methods can only be used under deterministic discharge conditions. The discharge current is variable in actual application practices, so estimating the SOH of LIBs at uncertain discharge conditions is very difficult without considering the random discharge current (Salinas and Kowal, 2020).

Nowadays both model-based and data-driven methods have been applied to estimate the SOH of LIBs considering random discharge conditions. The model-based methods used equivalent circuit models

[1]School of Electrical and Control Engineering, North University of China, Taiyuan 030051, China

[2]School of Data Science and Technology, North University of China, Taiyuan 030051, China

[3]Lead contact

*Correspondence: jiajianfang@nuc.edu.cn

https://doi.org/10.1016/j.isci.2022.103988

(ECM) (Bian et al., 2020) or electrochemical models (EM) (Xiong et al., 2017) to establish the corresponding state-space equation or fitting formula of the battery degradation process. Because the model parameters are complicated, these methods require the development of a battery degradation model with a balance between accuracy and complexity. The data-driven methods do not need to consider the battery's complex aging mechanism or electrochemical reaction. They extract the implicit information on the battery health status from a wide variety of experimental datasets to perform SOH prediction. Various machine learning (ML) algorithms are employed to learn the relationship between the battery health indicators (HIs) and SOH. Direct health indicators (DHIs) include battery capacity and internal resistance, which are the most obvious characteristics of battery degradation. Richardson et al. (Richardson et al., 2017) used multi-output Gaussian process regression (GPR) models to capture the battery capacity degradation trends for predicting SOH. Although it had effectively exploited data from identical batteries to improve forecasting performance, the capacity acquisition method is mainly the ampere-hour method based on the current at present, which has the cumulative errors in actual applications. Sepasi et al. (Sepasi et al., 2015) proposed a hybrid method combining Coulomb counting (CC) and extended Kalman filter (EKF) algorithm to derive the internal resistance of LIBs and then predict SOH. However, the internal resistance of a battery cannot be measured directly online, and it is easily disturbed by noise.

Therefore, indirect SOH estimation methods have also been proposed to predict the SOH of LIBs. They can learn nonlinear mappings between the battery SOH and indirect health indicators (IHIs) extracted from battery health information such as voltage, current, and temperature, which can be easily measured in the process of battery use (Jia et al., 2020; Yu et al., 2017). Tian et al. (Tian and Qin, 2021) extracted the discharge time, the voltage upward appreciation after discharge, and the variance of discharge voltage curve from random discharge data to predict the SOH of LIBs. Venugopal et al. (Venugopal and Vigneswaran, 2019) chose 18 IHIs from the change curve of discharge voltage, current, temperature, and time. However, too many IHIs resulted in redundant degradation information and a complex extraction process. Fan et al. (Fan et al., 2020) selected the observable variables such as charging voltage, current, and temperature as inputs to study the change of SOH. They reported that the constant-current-constant-voltage (CCCV) charging process was more peaceful and controllable than the random discharge process. The charging curve of CCCV mode can reflect the battery capacity under random discharge. But these IHIs were not artificially processed, so the SOH predictive accuracy was undesirable. Hence, selecting IHIs with high-quality and simple calculations remains a challenging problem.

Recently, deep learning (DL) and extreme learning machine (ELM) have gained popularity in natural language processing, time series forecasting, system modeling, etc. DL networks can automatically learn abstract features of multisource heterogeneous data by designing a complex multilayer neural network model, which brings the dawn of artificial intelligence research (Mu and Zeng, 2019). ELM is a single-hidden-layer feedforward neural network, where input weights and biases can be assigned independently without changing, and the output weight can be analytically determined by simple generalized inverse operation (Ding et al., 2014). In addition, ELM has better generalization performance and faster learning speed compared with backpropagation neural networks (BPNN). Fan et al. (Fan et al., 2020) developed a hybrid network of gate recurrent unit-convolutional neural network (GRU-CNN) for the battery SOH estimation, which can find the shared information from characteristic parameters of the battery and learn time dependencies of these parameters. Li et al. (Li et al., 2021) proposed a battery SOH estimation model of a recurrent neural network with a long short-term memory structure (LSTM-RNN) to overcome the limitation of the short memory of RNN. They pointed out that the model could play a powerful role in handling noisy inputs and did not require specific inputs. A hybrid gray wolf optimizer (HGWO) algorithm was used to optimize the key parameters of the Forgetting Online Sequential Extreme Learning Machine (FOS-ELM) for higher efficiency and accuracy (Fan et al., 2019).

However, the random generation of an input weight and the presence of only one hidden layer reduce the ability of ELM to learn typical features of the input data when faced with larger data. Although DL strategies have a stronger learning ability than ELM, the reverse fine-tuning process and multilayer network structure make the algorithm run slowly. Deep extreme learning machine (DELM) can use extreme learning machine-automatic encoder (ELM-AE) to initialize the input weights of each hidden layer and perform hierarchical unsupervised training without the reverse fine-tuning process, which is faster than the traditional DL strategy (Li et al., 2019). In addition, the prediction accuracy of DELM is higher than that of ELM (Tang et al., 2017). However, the current DELM lacks a mechanism to select the optimal key

Table 1. The specific operating environment of the battery

Battery no	RW discharge current	RW discharge duration
RW3, RW4, RW5	A randomized sequence of discharging currents between 0.5A and 4A	5 min
RW14	Be skewed toward selecting lower currents between 0.5A and 5A	1 min
RW20	Be skewed toward selecting higher currents between 0.5A and 5A	1 min

parameters, and the efficiency of online learning is low. As a result, it is necessary to find the optimal solution for these parameters and improve the weight learning efficiency of multilayer feed-forward networks.

The sparrow search algorithm (SSA) is superior to gray wolf optimizer (GWO) and particle swarm optimization (PSO) in terms of solution speed, stability, and convergence accuracy (Xue and Shen, 2020). Similar to other optimization algorithms, diversity loss of SSA's population in optimization procedures may cause local minima. Therefore, driven by the desire to improve the ability of SOH prediction accuracy, a deep extreme learning machine (DELM) optimized by the improved sparrow search algorithm (ISSA) is proposed to effectively estimate the battery SOH under the condition of random current discharge in this paper. The contributions and innovations of this paper are as follows:

1) Through the analysis of the random aging dataset, it is revealed that the battery's internal resistance and voltage standard deviation (SD) extracted from the small fragments of the random discharging voltage and current curve show an identical trend with the degraded battery capacity.
2) Two IHIs are extracted from the random partial discharging voltage and current data. They are internal resistance within a short time (IRWST) and voltage SD within a short time (VSDWST), respectively. IHIs are highly robust to random partial discharging data, which enables the proposed method to estimate battery SOH in random partial discharging conditions.
3) An improved SSA is proposed to optimize the input weights and biases of the DELM to effectively learn the nonlinear mapping between IHIs and the battery SOH. The improved SSA can expand the search space and speed up the movement of the population by utilizing the elite opposition-based learning (EOBL) and the Cauchy-Gaussian mutation operator. Experimental results demonstrate that the proposed method can obtain higher estimation accuracy and faster running speed compared with the combinations of other optimization algorithms and DELM.

RESULTS

As summarized in Table 1, this paper uses the experiment data of five batteries (identified as RW3, RW4, RW5, RW14, RW20) in a random battery aging dataset provided by NASA (Bole et al., 2014b). Here, the random current discharge of a battery is called random walk (RW). The experiment is performed with 18,650 LIBs whose nominal capacity is 2Ah and the cut-off voltage of charging and discharging are 4.2V and 3.2V, respectively. In an RW cycle, the CCCV strategy is adopted for charging, including the CC step at 2A until 4.2V and the CV step until 0.01A. Then the discharge rate is randomly selected from a predefined current set and each partial discharging cycle lasts for the same time until the battery discharges to the cut-off voltage. After every 50 RW cycles, two reference charge and discharge cycles are carried out to provide the real SOH. The reference charging process is the same as that of the RW experiment, but the discharge process uses constant current discharge. Further details about this battery dataset can be found in Ref (Bole et al., 2014a). Figure 1 shows the capacity degradation process of five batteries. The current and voltage curves of one reference charge-discharge experiment and one RW experiment of the battery RW3 are shown in Figure 2.

The internal resistance within a short time (IRWST) and the voltage SD within a short time (VSDWST) can be extracted from random partial discharging data for estimating battery SOH. The Pearson Correlation Coefficient (PCC) γ is used to mathematically prove the effectiveness of the extracted IHIs in indicating the battery capacity, and its formula is:

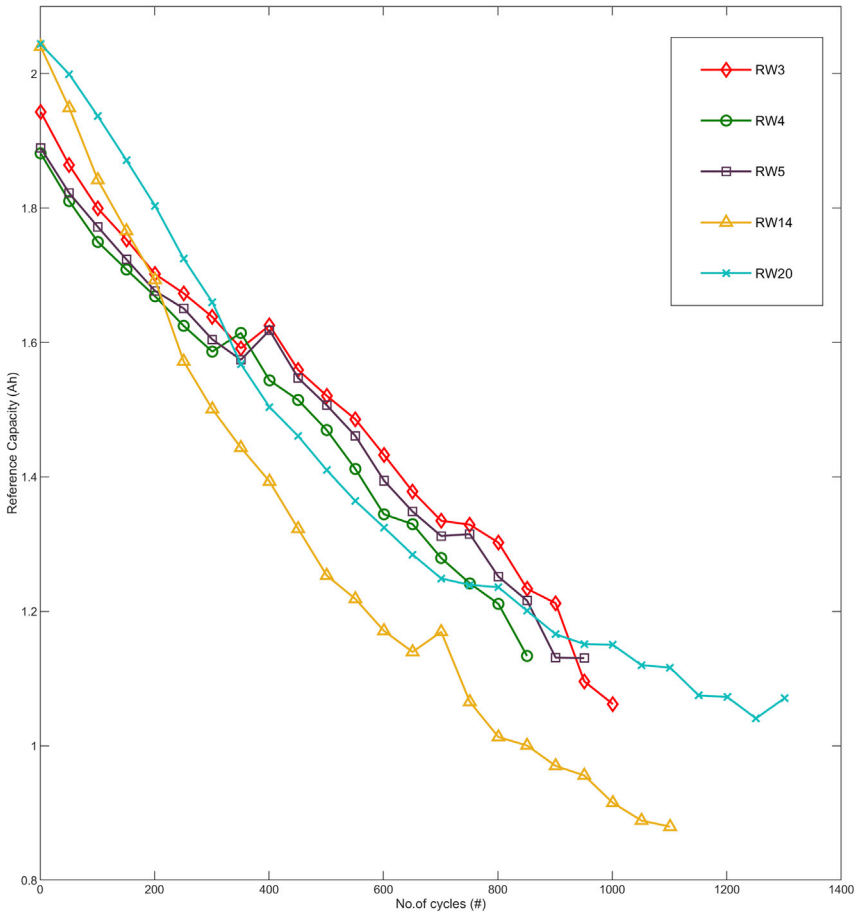

Figure 1. The attenuation curves of the battery reference capacity (Bole et al., 2014b)

$$\gamma = \frac{\sum_{i=1}^{n}(IHI_i - \overline{IHI})(C_i - \overline{C})}{\sqrt{\sum_{i=1}^{n}(IHI_i - \overline{IHI})^2}\sqrt{\sum_{i=1}^{n}(C_i - \overline{C})^2}} \quad \text{(Equation 2)}$$

where n is the number of the extracted IHI and the battery capacity; $\overline{IHI}$ and $\overline{C}$ are the average values of the IHI and the battery capacity, respectively. When the value γ is close to one or -1, it indicates that IHI has high linearity with the battery capacity. Tables 2 and 3 show the PCCs corresponding to different time intervals for IRWST and VSDWST of RW3 in different voltage windows, respectively.

The data extracted from the 4.2V–3.5V of the four batteries are integrated as a training dataset and the data extracted from the 4.2V–3.5V of the remaining battery is used as the testing dataset. The DELM network is constructed using three hidden layers, taking into account the fact that adding hidden layers complicates the network and increases training time. Experiments have shown that increasing the number of hidden layers to four increases the execution time of the algorithm by 2.48 times, but the RMSE is only reduced by 0.12%. To accurately predict the battery SOH, through repeatedly simulating trials, the number of nodes in the three hidden layers is determined to be 30, 20, and 10, respectively. The network activation function is the sigmoid function, and the Tikhonov regularization is set to 10^{12}. The population number, iteration times, percentage of discoverers, and warning value of SSA are 30, 80, 0.7, and 0.6, respectively. The SOH estimation results with different time intervals for five batteries are shown in Figure 3.

In practical applications, the battery may be recharged before it is completely exhausted, so it would be more practical to implement the proposed SOH estimation method under different RW partial discharging conditions. Therefore, the extraction of two IHIs and the ISSA-DELM algorithm are

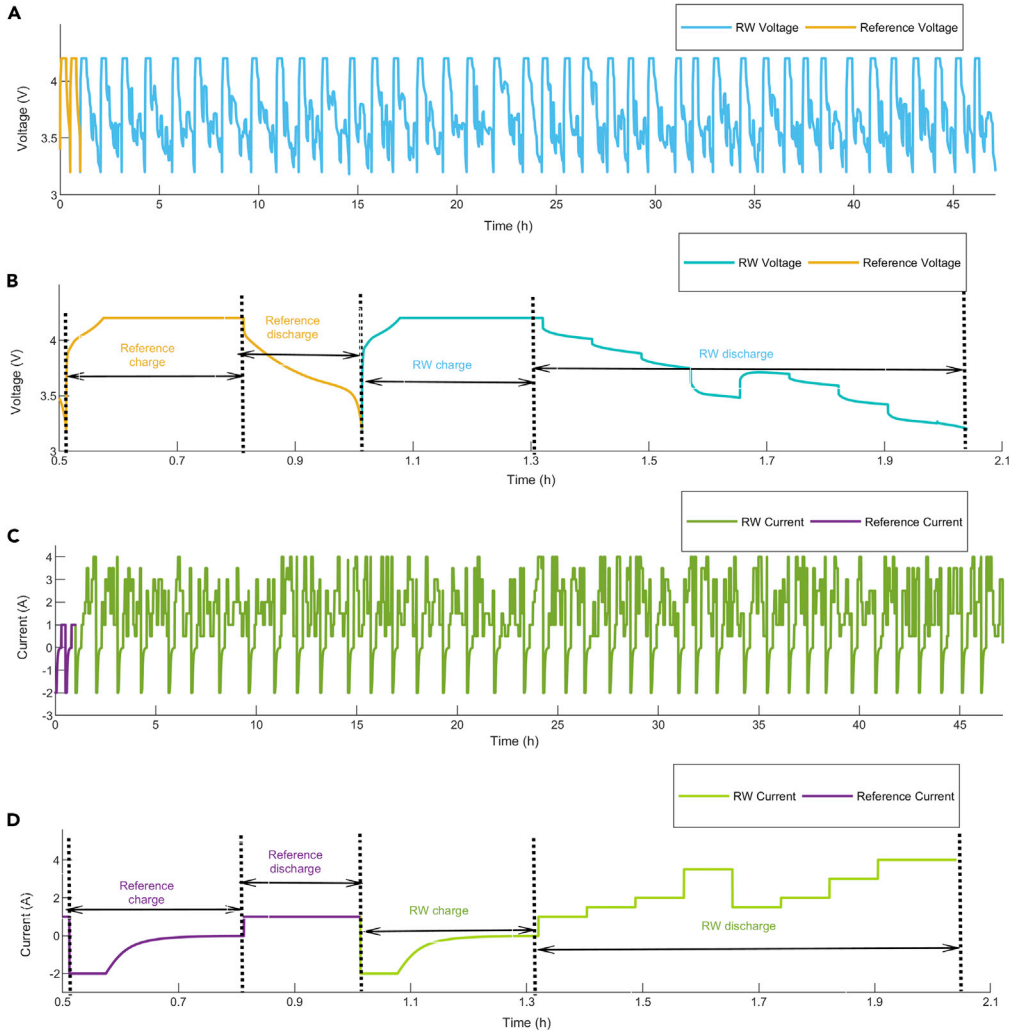

Figure 2. The current and voltage curves of the battery RW3

(A–D) (A) voltage of two reference charge and discharge cycles and 50 RW cycles, (B) voltage of one reference charge-discharge cycle and one RW cycle, (C) current of two reference charge-discharge cycles and 50 RW cycles, (D) current of one reference charge-discharge cycle and one RW cycle

performed under different voltage windows to evaluate the effectiveness of the proposed method in different practical discharging conditions. The overall estimated results of five batteries are given in Figure 4.

Furthermore, to explain the effectiveness of the SOH estimation based on the proposed method, the prediction results obtained in the 4.2V–3.5V voltage window are considered and compared with those of SSA-DELM, IGWO-DELM, and IPSO-DELM. IGWO is composed of gray wolf optimization (GWO) and differential evolution (DE) (Zhu et al., 2015), and IPSO is formed by merging particle swarm optimization (PSO) and genetic algorithm (GA) (Kao and Zahara, 2008). To make comparisons without deviations, the population size and iteration times of four optimization algorithms are set to 30 and 80, respectively. The upper and lower bounds of the scaling factor of IGWO are 0.2 and 0.8, respectively, and the crossover probability is 0.1. The inertia weight, crossover probability, and mutation probability of IPSO are 0.7, 0.7, and 0.3, respectively. SSA-DELM has the same parameters as ISSA-DELM. Figure 5 shows the SOH estimation results and the iterative convergence curve of fitness function of five batteries using four different methods. The RMSE and execution time of these methods are shown in Tables 4 and 5, respectively.

Table 2. PCC between IRWST and the battery capacity

Time intervals	4.2V–3.5V	4.2V–3.6V	4.2V–3.7V	4.2V–3.8V	4.2V–3.9V	4.2V–4.0V
5s	−0.993	−0.991	−0.989	−0.988	−0.987	−0.987
15s	−0.985	−0.984	−0.983	−0.984	−0.984	−0.990
30s	−0.983	−0.982	−0.981	−0.983	−0.987	−0.992

DISCUSSION

In this study, an indirect SOH estimation method based on ISSA-DDLM is proposed to predict the SOH of LIBs under random discharging conditions. In addition, the extracted IHIs must be highly correlated with battery capacity to estimate accurate SOH well.

As can be seen in Figure 1, the reference capacity decay rate for different RW discharge currents is various. Because the charging conditions of the five batteries are the same, it can be concluded that the difference in the reference capacity trend may be related to the difference in discharge current. Most of the existing research works only focus on the standard charging and discharging modes with many assumptions. Because the batteries are always used under random load conditions, the standard tests cannot be performed to measure the battery reference capacity and calculate SOH. Hence, it is usually necessary to indirectly predict the SOH based on the collected random discharge data.

From Figure 2, it can be seen that the random current is composed of several constant currents. Within a short period, the battery discharging current is static, and the discharging voltage changes because of the influence of internal resistance. Therefore, the IHIs related to the SOH can be extracted from those current and voltage curves within a short discharging interval. This paper extracts two IHIs called IRWST and VSDWST from random partial discharge data. The correlation coefficients between two IHIs and the battery capacity are shown in Tables 2 and 3, respectively.

It can be observed from Table 2 that for any given voltage window, a shorter time often results in a stronger correlation between IRWST and the battery capacity. Table 3 shows that under a particular voltage window, the linearity between VSDWST and the battery capacity is greatly affected by different time intervals. The shorter the time interval, the higher the relationship between VSDWST and battery capacity. Therefore, this paper chooses 5s as the time interval. It is important to point out that with the same time interval, different voltage windows are studied so that the extracted IHIs can be applied to different actual half-discharging environments. It can also be seen from Tables 2 and 3 that in each voltage window, the absolute values of the PCC of two IHIs extracted in 5s are all more than 0.980, which proves that there is a strong linear correlation between the capacity and each IHI. Therefore, high accuracy SOH estimations can be obtained by using these IHIs as model inputs.

As shown in Figure 3, when the IHIs are extracted within 5s, the SOH estimation curves of five batteries are exceedingly close to the actual SOH values, and the AEs are well limited under 3%. Especially for RW4 and RW5, their RMSEs are only 0.49 and 0.65%, respectively. Moreover, extending the time interval from 5s to 15s generally results in a greater RMSE, with a maximum increase of 1.2%. When the time interval is extended to 30s, the SOH estimation error is larger, and the maximum RMSE reaches 3.42%. Both of these phenomena are more evident for two batteries RW14 and RW20. This is because their random load switching time is one-fifth of the random load switching time of the other three batteries, and there is a large difference between the IHIs and the battery capacity. These results confirm that IHIs extracted within 5s have the highest correlation with the battery capacity, under an ideal scenario that 4.2V–3.5V discharging curves are available. Thus, it is a good choice to extract the battery's internal resistance and voltage SD within 5s.

Table 3. PCC between VSDWST and the battery capacity

Time intervals	4.2V–3.5V	4.2V–3.6V	4.2V–3.7V	4.2V–3.8V	4.2V–3.9V	4.2V–4.0V
5s	−0.982	−0.983	−0.981	−0.982	−0.982	−0.990
15s	−0.972	−0.968	−0.967	−0.969	−0.969	−0.966
30s	−0.964	−0.956	−0.955	−0.958	−0.961	−0.969

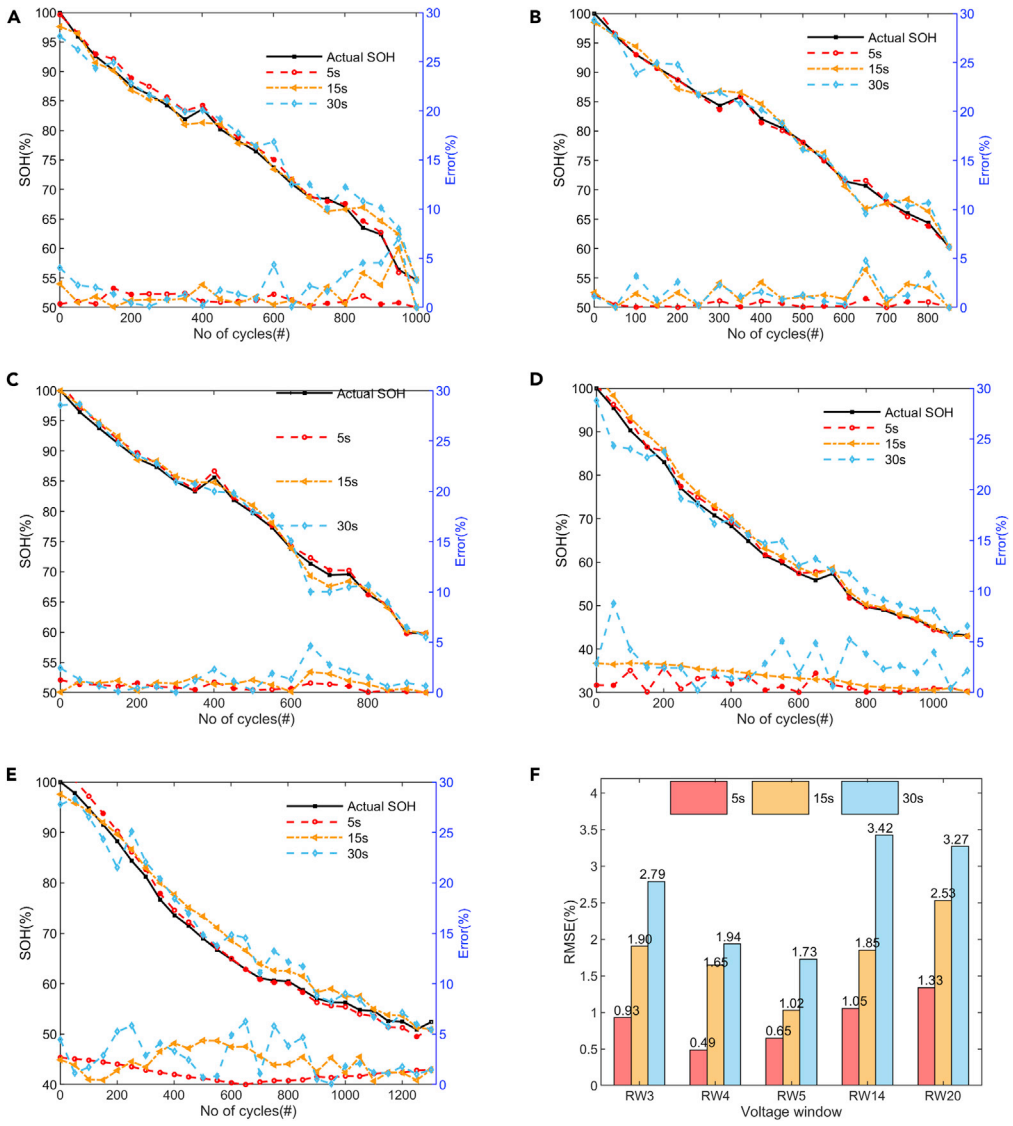

Figure 3. The SOH estimation results with different time intervals for the five batteries

(A–F) (A) SOH estimation result of RW3, (B) SOH estimation result of RW4, (C) SOH estimation result of RW5, (D) SOH estimation result of RW14, (E) SOH estimation result of RW20, (F) Histogram of RMSE for different time intervals for five batteries

Figure 4A illustrates the deviation of the estimated SOH from the actual SOH at various voltage windows and MAE value to quantify the deviation. The maximum MAE of 1.01% is achieved when the voltage window is 4.2V–4.0V, whereas the minimum MAE of 0.70% occurs when the voltage window is 4.2V–3.8V. When the voltage window is shortened to 4.2V–3.5V and below, the MAE are all within 1.01%, indicating that the proposed SOH estimation method can be extended to different local RW discharge conditions with high prediction accuracy.

The relationship between the SOH estimation accuracy and the voltage window is shown in Figure 4B. As can be seen from Figure 4B, the proposed method can generally guarantee satisfactory accuracy under different voltage windows, and the RMSE of each battery can be well limited in the range of 0.17–2.15%. The accuracy of the SOH estimate is slightly reduced only when the battery RW20 is used as the testing battery. This can be explained by the RW20 degradation tendency to choose a higher current compared to the other four batteries. Within the same discharge window, the IHIs of RW20 have relatively low linear correlation with the battery capacity. In terms of the voltage window, the average RMSEs show that the voltage window

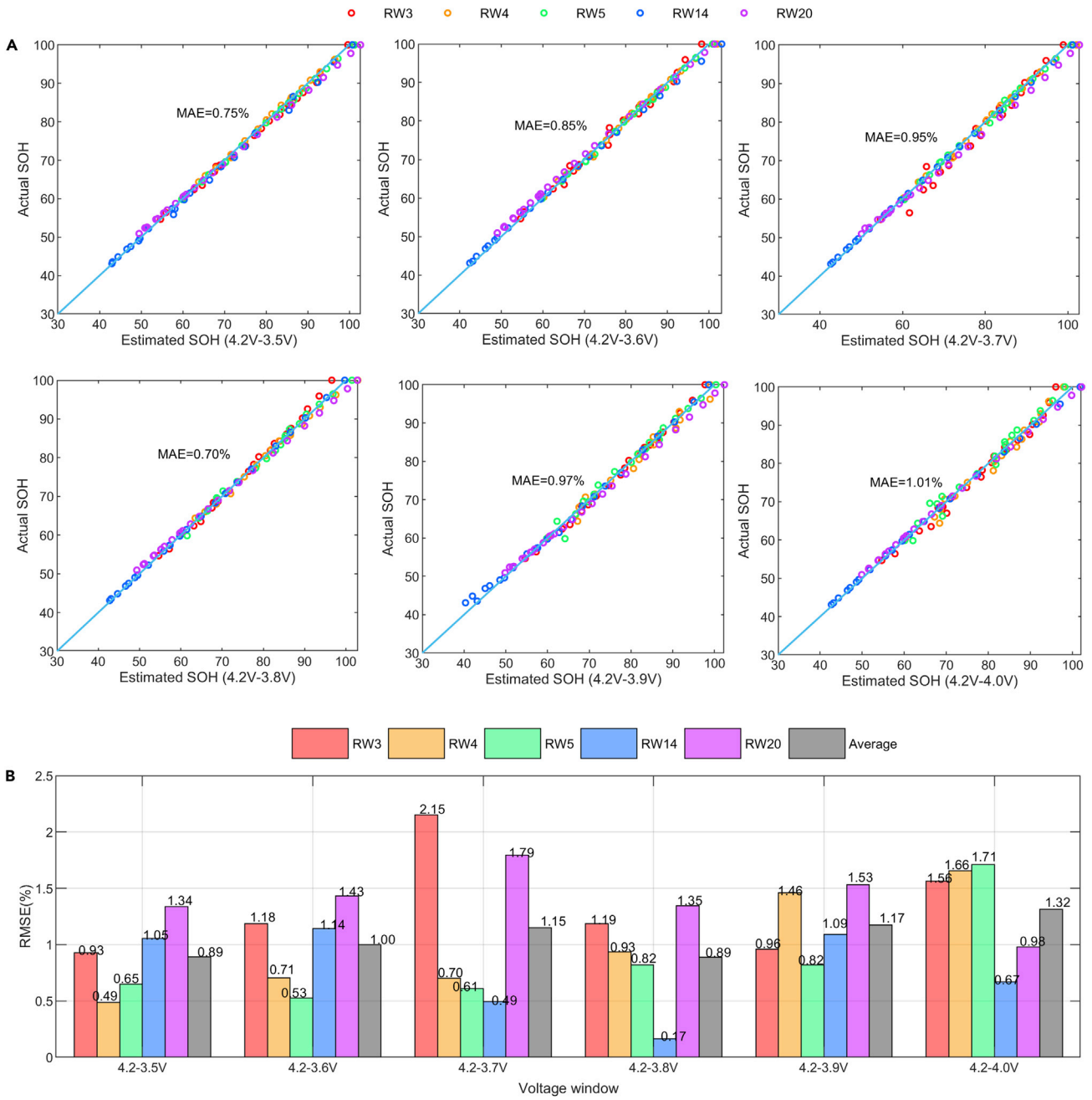

Figure 4. The overall estimated results of five batteries

(A and B) (A) estimated and actual values for various voltage windows, the blue straight line indicates zero deviation between estimated and actual values, (B) RMSEs for each testing battery, and average RMSE for five batteries with different voltage windows

has less effect on the accuracy of the SOH estimation. Across the five different voltage windows, the average RMSE is well limited from 0.89% to 1.32%, indicating that these voltage ranges provide sufficient information to indicate the SOH. Consequently, the ISSA-DELM-based indirect SOH estimation method can be simply and accurately applied to partial random discharging conditions.

Comparing the SOH estimation curves of other methods, it can be seen from Figure 5 that the prediction error of SSA-DELM is always the largest. Among the SOH prediction results of five batteries, the ISSA-DELM algorithm can track the changing tendency of the battery SOH well, and the error is smaller

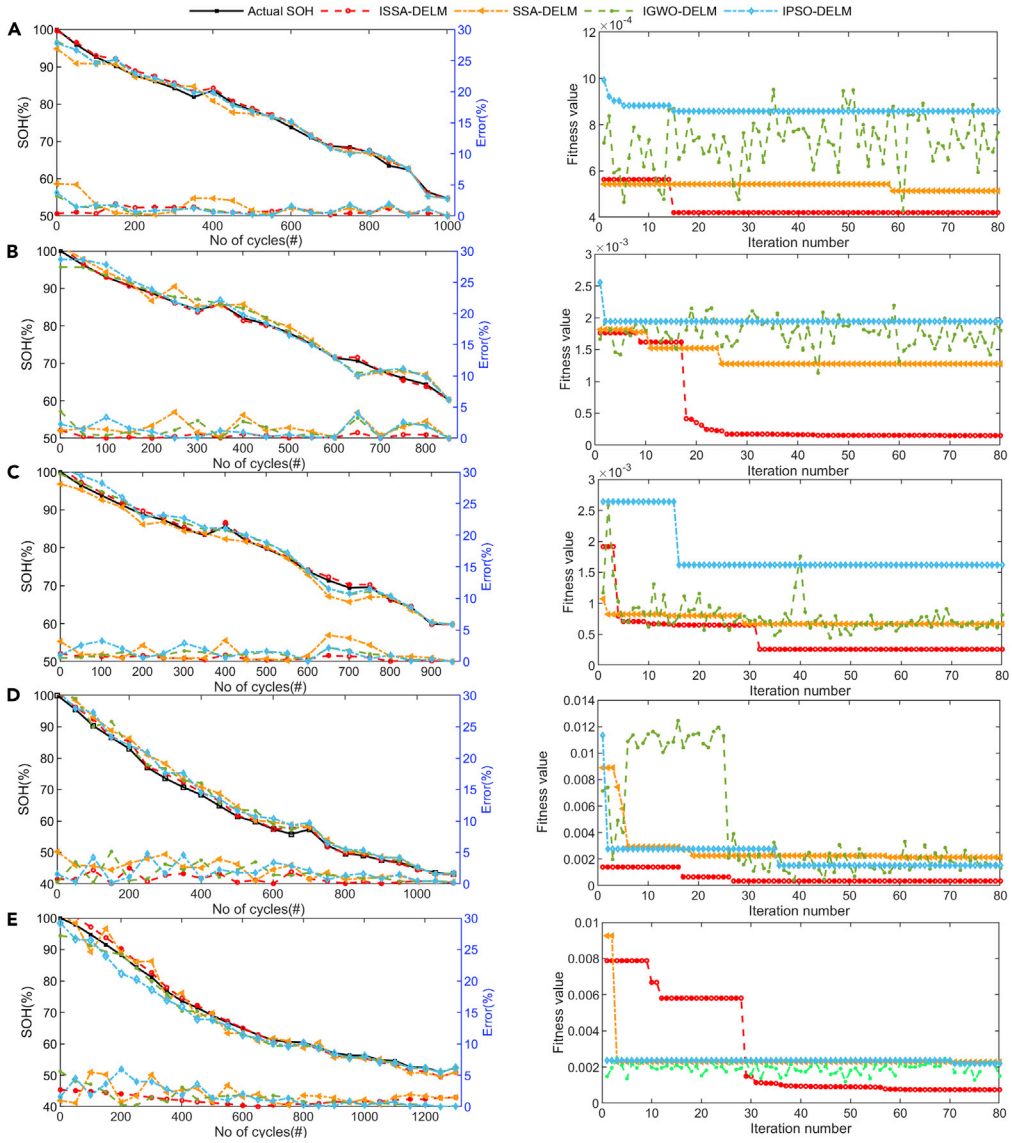

Figure 5. The comparison among different models for five batteries

(A–E) (A) SOH estimation result of RW3, (B) SOH estimation result of RW4, (C) SOH estimation result of RW5, (D) SOH estimation result of RW14, (E) SOH estimation result of RW20

than the other algorithms. The main reason for this phenomenon is that EOBL and Cauchy-Gaussian mutation operators can increase the population diversity of the SSA algorithm to some extent and prevent the algorithm from prematurely converging and falling into the local optimization. The ISSA algorithm converges faster than the IGWO algorithm, but its convergence speed is not as fast as that of the IPSO and SSA algorithms. However, the ISSA algorithm can jump out of the local optimization and reduce the

Table 4. RMSE (%) of different methods

Method	RW3	RW4	RW5	RW14	RW20
ISSA-DELM	0.93	0.49	0.65	1.05	1.34
SSA-DELM	2.03	2.06	1.90	2.63	2.35
IGWO-DELM	1.26	1.69	1.15	2.08	1.90
IPSO-DELM	1.33	1.75	1.62	2.21	2.14

Table 5. Execution time (s) of different methods

Method	RW3	RW4	RW5	RW14	RW20
ISSA-DELM	8.77	8.63	9.07	8.75	8.53
SSA-DELM	6.50	6.57	6.55	6.11	6.49
IGWO-DELM	13.60	13.97	13.13	13.91	13.60
IPSO-DELM	13.49	13.41	13.15	13.87	13.06

prediction error of the DELM neural network, which is a trade-off between the fast convergence speed and low residual error simultaneously. As can be seen from Figure 5C, the ISSA algorithm starts to converge quickly at the 18th iteration. As the number of iterations increases, the algorithm can jump out of the local optimization, and finally find the global optimal solution in the 34th iteration. On the contrary, the SSA algorithm started to converge at the 28th iteration and fell into the local optimization. Similarly, the IPSO algorithm also tends to converge prematurely and fall into the local optimization. Although the IGWO algorithm can jump out of the local optimization, its optimization performance is volatile and the fitness function curve fluctuates significantly.

Tables 4 and 5 summarize the RMSE and execution time of four methods, respectively. It can be found from Table 4 that the RMSE of ISSA-DELM is smaller than that of the other three methods, indicating that the combination of ISSA and DELM neural network can more accurately capture the nonlinear mapping between two IHIs and the SOH, and the proposed algorithm is more accurate than the other optimization algorithms in terms of convergence accuracy. Table 5 shows that the ISSA-DELM algorithm runs about half as long as the IPSO-DELM and IGWO-DELM algorithms. This is primarily because EOBL uses only elite individuals to search the current search space and mapping space in parallel. Compared to the DE or GA algorithm, this can reduce the time spent on each iteration of the optimization algorithm to some extent.

Conclusions

Because the battery capacity cannot be obtained through online measurement in actual applications, it is also a challenging problem to estimate the SOH of LIBs under random discharging conditions. A deep extreme learning machine (DELM) optimized by the improved sparrow search algorithm (ISSA) is presented to effectively estimate the battery SOH. Two indirect health indicators (IHIs), named internal resistance within a short time (IRWST) and voltage SD within a short time (VSDWST), are extracted from random partial discharging data. Then, the EOBL algorithm and the Cauchy–Gaussian mutation strategy are applied to increase the diversity of sparrow populations and prevent the SSA algorithm from falling into the local optimization. Finally, the key parameters of DELM are optimized utilizing the improved SSA algorithm, and an ISSA-DELM model is constructed to carry on the SOH estimation. Long-term cycling tests of five batteries with different random discharging currents have been employed to verify the effectiveness of the proposed method. Even if the random discharging voltage window is very small from 4.2V to 4.0V, the RMSE can be well limited under 1.71%. Hence, the ISSA-DELM algorithm has higher prediction accuracy than the other three algorithms SSA-DELM, IGWO-DELM, and IPSO-DELM, while maintaining a short running time.

Limitations of the study

This method can be utilized to estimate the SOH of LIBs under partially random discharge conditions. However, the selected IHIs were only extracted from the voltage and current data. Because the temperature variation during the battery charge and discharge also affects the SOH, it is necessary to further study the temperature profile to obtain more information for characterizing the battery SOH. Furthermore, the method is only validated using NASA's random battery aging dataset. In many applications, such as electric vehicles, the use of random loads is very complex and irregular, so the prediction method should be further validated using actual operating data.

STAR★METHODS

Detailed methods are provided in the online version of this paper and include the following:

- KEY RESOURCES TABLE

SUPPLEMENTAL INFORMATION

Supplemental information can be found online at https://doi.org/10.1016/j.isci.2022.103988.

ACKNOWLEDGMENTS

The authors gratefully acknowledge the Natural Science Foundation of China (No. 72071183), the Research Project Supported by Shanxi Scholarship Council of China (No. 2020-114), and the Natural Science Foundation of Shanxi Province (No. 201901D111164).

AUTHOR CONTRIBUTIONS

Conceptualization, S.Y. and J.J.; Writing – Original Draft, S.Y.; Revision, J.J., S.Y., Y.S., J.W., and X.P.; Supervision, J.Z.; Funding Acquisition, J.J. and J.Z.

DECLARATION OF INTERESTS

The authors declare no competing interests. The authors have no commercial or associative interests that might influence the work reported in this paper.

Received: July 19, 2021
Revised: December 15, 2021
Accepted: February 23, 2022
Published: April 15, 2022

REFERENCES

Bian, X., Liu, L., Yan, J., Zou, Z., and Zhao, R. (2020). An open circuit voltage-based model for state-of-health estimation of lithium-ion batteries: model development and validation. J. Power Sourc. *448*, 227401. https://doi.org/10.1016/j.jpowsour.2019.227401.

Bole, B., Kulkarni, C., and Daigle, M. (2014a). Adaptation of an Electrochemistry-Based Li-Ion Battery Model to Account for Deterioration Observed under Randomized Use (Annual Conference of the Prognostics and Health Management Society; 2014).

Bole, B., Kulkarni, C., and Daigle, M. (2014b). Randomized Battery Usage Data Set. NASA Ames Prognostics Data Repository (NASA Ames Research Center). http://ti.arc.nasa.gov/project/prognosticdata-repository.

Ding, S.F., Xu, X.Z., and Nie, R. (2014). Extreme learning machine and its applications. Neural Comput. Appl. *25*, 549–556. https://doi.org/10.1007/s00521-013-1522-8.

Fan, J.M., Fan, J.P., Liu, F., Qu, J.T., and Li, R.F. (2019). A novel machine learning method based approach for Li-ion battery prognostic and health management. IEEE Access *7*, 160043–160061. https://doi.org/10.1109/access.2019.2947843.

Fan, Y.X., Xiao, F., Li, C.R., Yang, G.R., and Tang, X. (2020). A novel deep learning framework for state of health estimation of lithium-ion battery. J. Energ. Storage *32*, 101741. https://doi.org/10.1016/j.est.2020.101741.

Huang, K., Zhou, Y., Wu, X., and Luo, Q. (2016). A cuckoo search algorithm with elite opposition-based strategy. J. Intell. Syst. *25*, 567–593. https://doi.org/10.1515/jisys-2015-0041.

Hussain, D., Khan, M.A., Abbas, S., Naqvi, R.A., Mushtaq, M.F., Rehman, A., and Nadeem, A. (2021). Enabling smart cities with cognition based intelligent route decision in vehicles empowered with deep extreme learning machine. Cmc-Computers Mater. Continua *66*, 141–156. https://doi.org/10.32604/cmc.2020.013458.

Jia, J., Liang, J., Shi, Y., Wen, J., Pang, X., and Zeng, J. (2020). SOH and RUL prediction of lithium-ion batteries based on Gaussian process regression with indirect health indicators. Energies *13*, 375. https://doi.org/10.3390/en13020375.

Jia, J.F., Wang, K.K., Shi, Y.H., Wen, J., Pang, X.Q., and Zeng, J.C. (2021a). A multi-scale state of health prediction framework of lithium-ion batteries considering the temperature variation during battery discharge. Journal of Energy Storage *42*, 103076. https://doi.org/10.1016/j.est.2021.103076.

Jia, J.F., Wang, K.K., Pang, X.Q., Shi, Y.H., Wen, J., and Zeng, J.C. (2021b). Multi-scale prediction of RUL and SOH for lithium-ion batteries based on WNN-UPF combined model. Chin. J. Electronics *30*, 26–35. https://doi.org/10.1049/cje.2020.10.012.

Kao, Y.T., and Zahara, E. (2008). A hybrid genetic algorithm and particle swarm optimization for multimodal functions. Appl. Soft Comput. *8*, 849–857. https://doi.org/10.1016/j.asoc.2007.07.002.

Kim, T., Song, W., Son, D.-Y., Ono, L.K., and Qi, Y. (2019). Lithium-ion batteries: outlook on present, future, and hybridized technologies. J. Mater. Chem. A *7*, 2942–2964. https://doi.org/10.1039/c8ta10513h.

Li, C.S., Zhang, N., Lai, X.J., Zhou, J.Z., and Xu, Y.H. (2017). Design of a fractional-order PID controller for a pumped storage unit using a gravitational search algorithm based on the Cauchy and Gaussian mutation. Inf. Sci. *396*, 162–181. https://doi.org/10.1016/j.ins.2017.02.026.

Li, K., Xiong, M., Li, F., Su, L., and Wu, J. (2019). A novel fault diagnosis algorithm for rotating

machinery based on a sparsity and neighborhood preserving deep extreme learning machine. Neurocomputing *350*, 261–270. https://doi.org/10.1016/j.neucom.2019.03.084.

Li, W., Sengupta, N., Dechent, P., Howey, D., Annaswamy, A., and Sauer, D.U. (2021). Online capacity estimation of lithium-ion batteries with deep long short-term memory networks. J. Power Sourc. *482*, 228863. https://doi.org/10.1016/j.jpowsour.2020.228863.

Luo, M.N., Zhang, L.L., Liu, J., Guo, J., and Zheng, Q.H. (2017). Distributed extreme learning machine with alternating direction method of multiplier. Neurocomputing *261*, 164–170. https://doi.org/10.1016/j.neucom.2016.03.112.

Mu, R.H., and Zeng, X.Q. (2019). A review of deep learning research. Ksii Trans. Internet Inf. Syst. *13*, 1738–1764. https://doi.org/10.3837/tiis.2019.04.001.

Panchal, S., Mathew, M., Fraser, R., and Fowler, M. (2018). Electrochemical thermal modeling and experimental measurements of 18650 cylindrical lithium-ion battery during discharge cycle for an EV. Appl. Therm. Eng. *135*, 123–132. https://doi.org/10.1016/j.applthermaleng.2018.02.046.

Pang, X., Huang, R., Wen, J., Shi, Y., Jia, J., and Zeng, J. (2019). A lithium-ion battery RUL prediction method considering the capacity regeneration phenomenon. Energies *12*, 2247. https://doi.org/10.3390/en12122247.

Qu, B.Y., Lang, B.F., Liang, J.J., Qin, A.K., and Crisalle, O.D. (2016). Two-hidden-layer extreme learning machine for regression and classification. Neurocomputing *175*, 826–834. https://doi.org/10.1016/j.neucom.2015.11.009.

Richardson, R.R., Osborne, M.A., and Howey, D.A. (2017). Gaussian process regression for forecasting battery state of health. J. Power Sourc. *357*, 209–219. https://doi.org/10.1016/j.jpowsour.2017.05.004.

Rosa Palacin, M. (2018). Understanding ageing in Li-ion batteries: a chemical issue. Chem. Soc. Rev. *47*, 4924–4933. https://doi.org/10.1039/c7cs00889a.

Saha, B., Goebel, K., Poll, S., and Christophersen, J. (2009). Prognostics methods for battery health monitoring using a Bayesian framework. IEEE Trans. Instrumentation Meas. *58*, 291–296. https://doi.org/10.1109/tim.2008.2005965.

Salinas, F., and Kowal, J. (2020). Discharge rate capability in aged Li-ion batteries. J. Electrochem. Soc. *167*, 140519. https://doi.org/10.1149/1945-7111/abc207.

Sepasi, S., Ghorbani, R., and Liaw, B.Y. (2015). Inline state of health estimation of lithium-ion batteries using state of charge calculation. J. Power Sourc. *299*, 246–254. https://doi.org/10.1016/j.jpowsour.2015.08.091.

Tang, J., Deng, C., and Huang, G.-B. (2017). Extreme Learning Machine for Multilayer Perceptron (IEEE), pp. 809–821. https://doi.org/10.1109/TNNLS. 2015.2424995.

Tian, H., and Qin, P. (2021). State of health prediction for lithium-ion batteries with a novel online sequential extreme learning machine method. Int. J. Energ. Res. *45*, 2383–2397. https://doi.org/10.1002/er.5934.

Tizhoosh, H.R. (2005). Opposition-based learning: a new scheme for machine intelligence. In Proceedings of the International Conference on Computational Intelligence for Modelling, Control and Automation (CIMCA '05) and International Conference on Intelligent Agents, Web Technologies and Internet Commerce (IAWTIC '05) (IEEE), pp. 695–701.

Tubishat, M., Abushariah, M.A.M., Idris, N., and Aljarah, I. (2019). Improved whale optimization algorithm for feature selection in Arabic sentiment analysis. Appl. Intelligence *49*, 1688–1707. https://doi.org/10.1007/s10489-018-1334-8.

Venugopal, P., and Vigneswaran, T. (2019). State-of-Health estimation of Li-ion batteries in electric vehicle using IndRNN under variable load condition. Energies *12*, 4338. https://doi.org/10.3390/en12224338.

Xie, S., Ren, L., Yang, X., Wang, H., Sun, Q., Chen, X., and He, Y. (2020). Influence of cycling aging and ambient pressure on the thermal safety features of lithium-ion battery. J. Power Sourc. *448*, 227425. https://doi.org/10.1016/j.jpowsour.2019.227425.

Xiong, R., Tian, J.P., Mu, H., and Wang, C. (2017). A systematic model-based degradation behavior recognition and health monitoring method for lithium-ion batteries. Appl. Energ. *207*, 372–383. https://doi.org/10.1016/j.apenergy.2017.05.124.

Xue, J., and Shen, B. (2020). A novel swarm intelligence optimization approach: sparrow search algorithm. Syst. Sci. Control Eng. *8*, 22–34. https://doi.org/10.1080/21642583.2019.1708830.

Yang, Y.R., Wen, J., Shi, Y.H., and Zeng, J.C. (2021). State of health prediction of lithium-ion batteries based on the discharge voltage and temperature. Electronics *10*, 1497. https://doi.org/10.3390/electronics10121497.

Yu, J.S., Mo, B.H., Tang, D.Y., Yang, J., Wan, J.Q., and Liu, J.J. (2017). Indirect state-of-health estimation for lithium-ion batteries under randomized use. Energies *10*, 2012. https://doi.org/10.3390/en10122012.

Zhang, S., Luo, Q., and Zhou, Y. (2017). Hybrid grey wolf optimizer using elite opposition-based learning strategy and simplex method. Int. J. Comput. Intelligence Appl. *11*, 1750012. https://doi.org/10.1142/S1469026817500122.

Zhu, A.J., Xu, C.P., Li, Z., Wu, J., and Liu, Z.B. (2015). Hybridizing grey wolf optimization with differential evolution for global optimization and test scheduling for 3D stacked SoC. J. Syst. Eng. Electronics *26*, 317–328. https://doi.org/10.1109/jsee.2015.00037.

STAR★METHODS

KEY RESOURCES TABLE

REAGENT or RESOURCE	SOURCE	IDENTIFIER
Deposited data		
"Randomized Battery Usage Data Set", NASA Ames Prognostics Data Repository	Bole et al., 2014a, 2014b	http://ti.arc.nasa.gov/project/prognosticdata-repository

RESOURCE AVAILABILITY

Lead contact

Further requests for information should be directed and will be handled by the corresponding author and lead contact, Jianfang JIA, email: jiajianfang@nuc.edu.cn.

Materials availability

This study did not generate new materials.

Data and code availability

- The dataset that informed or guided this study are available online.
- This paper does not report original code. Any additional information for reanalyzing this work is available from the lead contact upon request.

METHOD DETAILS

The proposed approach consists of IHIs extraction, DELM model, ISSA algorithm, explained in detail in this section.

IHIs extraction

By the mechanism analysis and the geometric analysis of RW discharging curves, two IHIs IRWST and VSDWST are extracted for performing the SOH estimation. The extraction process of IHIs using the battery RW3 is an example in the paper.

The internal resistance within a short time (IRWST)

As the battery ages, the internal resistance of the battery usually increases. When the current flows through the battery, its operating voltage drops due to the interference of the internal resistance. Since the discharge current is static in a short time, and the internal resistance of the battery increases, the internal resistance in a short time can be used as a health indicator for indicating the health of the battery. Taking RW3 as an example, Figure S1A shows the extraction process of IRWST. The specific calculation formula is as follows.

$$IRWST_i = \frac{V_{start} - V^i_{stop}}{I^i_{stop}} = \frac{V_{start} - V^i_{start+T}}{I^i_{stop}} \quad \text{(Equation 3)}$$

Among them, V_{start} represents the given start voltage, T refers to the given time interval in seconds, V^i_{stop} and I^i_{stop} are the voltage and current corresponding to the stop voltage of the *ith* RW cycle, respectively. Figure S1C shows changes in the proposed IRWST within 5s under different starting voltages. The degraded capacity ΔC is also given to show the identical trend between IRWST and degraded capacity, which is defined as

$$\Delta C = C_0 - C_t \quad \text{(Equation 4)}$$

Since the voltage drops quickly after being lower than 3.5V, there is a phenomenon that battery health information cannot be captured in a specific short time, so Figure S1C only shows the result of extracting IRWST from the starting voltage 3.55V to 4.2V. As shown in Figure S1C, as the battery ages, the IRWST

shows an increasing trend at different voltage levels, which is consistent with the trend of degraded capacity. In practical applications, most lithium-ion batteries are recharged before randomly discharging to the cut-off voltage, so the selected IHIs are expected to have a high robustness to the discharging partialness. By calculating the average IRWST of the voltage interval 0.05V for a given voltage window, an indirect health indicator related to this half-discharge window can be extracted to indicate the battery capacity. To show clearly and intuitively the correlation, the correlations between extracted results in the 4.2V–3.5V voltage window and the reference capacities of five batteries are visualized in Figure S1E, where IRWST and the battery capacity are normalized between 0 and 1, respectively. The blue straight line represents the best correlation between the battery reference capacity and IHI. In Figure S1E, the points are scattered from the upper left corner to the lower right corner, so IRWST and the battery capacity are negatively correlated. The points are distributed near the blue straight line, indicating that IRWST has a relatively strong correlation with the battery capacity.

The voltage standard deviation within a short time (VSDWST)

When the current passes through the battery, the working voltage of the battery will decrease due to the influence of the internal resistance of the battery. Moreover, under the condition of high current discharge, the electrode polarization enhances, the internal resistance increases and the discharge voltage decreases rapidly. Correspondingly, in low-speed discharge, the discharge voltage decreases slowly due to the relatively small internal resistance. Thus, VSDWST can be used to indicate SOH. The extraction process of VSDWST is shown in Figure S1B, which can be computed as

$$VSDWST_i = std\left(V_{\text{stop}}, V_{\text{stop}}\right) = \sqrt{\frac{1}{T+1}\left(\left(V_{\text{start}} - \overline{V_i}\right)^2 + \cdots + \left(V^i_{\text{stop}} - \overline{V_i}\right)^2\right)} \quad \text{(Equation 5)}$$

where $\overline{V_i}$ is the average voltage within T time intervals of the *ith* random discharging cycle. Figure S1D illustrates the VSDWST within 5 seconds at different starting voltages. It is shown in Figure S1D that the trend of VSDWST and the degraded capacity under different voltage levels is roughly the same. Similar to IRWST, VSDWST with the same voltage interval of 0.05V is extracted to investigate its effectiveness on the RW partial discharging data. Figure S1F is a scatter plot of normalized reference capacity and normalized VSDWST extracted in the voltage window 4.2V–3.5V. It can be seen from Figure S1F that the correlation between VSDWST and the battery reference capacity is relatively high when the battery voltage drops by 0.7V.

DELM model

The DELM overlaps multi-layer extreme learning machine-automatic encoder (ELM-AE) to form a deep neural network, which has a better predictive effect than a single-layer ELM algorithm (Luo et al., 2017). Moreover, the connection weights between the hidden layer and the output layer are determined by the time-efficient least-squares method (Qu et al., 2016). The output weight is obtained by minimizing the mean square error (MSE) during the training process. Therefore, it has a fast-training speed and excellent generalization performance. DELM can be formulated as (Hussain et al., 2021),

$$P = F\left(WA + 1^T \otimes B\right) \quad \text{(Equation 6)}$$

$$Y_P = \beta P \quad \text{(Equation 7)}$$

$$E = Y_t - Y_P = Y_t - \beta P \quad \text{(Equation 8)}$$

$$\beta = Y_t P^T \left(PP^T\right)^{-1} \quad \text{(Equation 9)}$$

where F represents the activation function of the network, a sigmoid function is chosen as the activation function so that its output is between 0 and 1. A is a combinatorial sequence of two IHIs. W, B, β, P are input weights, the biases of the hidden nodes, the output weight, and the result value of hidden nodes, respectively. In DELM, the output weight β is updated by constantly decreasing the evaluation error (E) of the model. And if E is close to zero, the prediction effect of DELM is best. Besides, to avoid overfitting, the famous Tikhonov regularization can be used to change Equation (9) into

$$\beta = YP^T \left(PP^T + v_0^2 I\right)^{-1} \quad \text{(Equation 10)}$$

where $v_0^2 > 0$ signifies the regularization term.

ISSA algorithm

Because the input weights and the biases of the DELM neural network are randomly addressed, which will reduce the accuracy of the battery's SOH prediction. In this paper, the improved sparrow search algorithm (ISSA), which combines elite opposition-based learning (EOBL), Cauchy-Gaussian mutation strategy, and sparrow search algorithm (SSA), is applied to optimize the key parameters of DELM.

SSA is one of the newly metaheuristic algorithms, which consists of producers, entrants, and scouters. Producers are responsible for finding food for whole sparrow populations. Then, scroungers decide whether to snatch the discoverer's food according to the food source quality. In addition, a few individuals are selected as scouters and their task is to randomly find new foraging sites. This discovering and tracking mode enables the SSA to have a high convergence speed and the ability to jump out of the local optimality. And their locations are updated as follows:

$$X_{i,j}^{t+1} = \begin{cases} X_{i,j}^{t} \cdot \exp\left(-\dfrac{i}{\alpha \cdot iter_{\max}}\right) & \text{if } R_2 < ST \\ X_{i,j}^{t} + Q \cdot L & \text{if } R_2 \geq ST \end{cases} \quad \text{(Equation 11)}$$

$$E_{i,j}^{t+1} = \begin{cases} Q \cdot \exp\left(\dfrac{X_{\text{worst}}^{t} - X_{i,j}^{t}}{i^2}\right) & \text{if } i > n/2 \\ X_{P}^{t+1} + \left|X_{i,j}^{t} - X_{P}^{t+1}\right| \cdot A^{+} \cdot L & \text{otherwise} \end{cases} \quad \text{(Equation 12)}$$

$$C_{i,j}^{t+1} = \begin{cases} X_{\text{best}}^{t} + \beta \cdot \left|X_{i,j}^{t} - X_{\text{best}}^{t}\right| & \text{if } f_i > f_g \\ X_{i,j}^{t} + P \cdot \left(\dfrac{\left|X_{i,j}^{t} - X_{\text{worst}}^{t}\right|}{(f_i - f_w) + \varepsilon}\right) & \text{if } f_i = f_g \end{cases} \quad \text{(Equation 13)}$$

$$A^{+} = A^{T}\left(AA^{T}\right)^{-1} \quad \text{(Equation 14)}$$

$$f = \frac{\sum_{i=1}^{n}\left(y_p(i) - y_t(i)\right)^2}{n} \quad \text{(Equation 15)}$$

where X,E,C are the locations of producers, entrants, and scouters, respectively, which are potential solutions for optimal input weights and hidden layer node bias of DELM neural networks. The fitness function f is calculated by the mean absolute error (MSE) between the predicted SOH y_p and the actual SOH y_t for evaluating the quality of potential optimal parameters. R_2 and ST are the early warning index and safety index that help producers efficiently search for the optimal solutions. $X_{i,j}$ represents the position of the ith sparrow in the jth dimension solution space. X_p, X_{worst}, X_{best} refer to the best position occupied by producers, the worst position of the whole sparrows, and the best position of the whole sparrows, respectively. If $i \leq n/2$, it denotes that the ith entrant is around to the optimal parameters of DELM; while $i > n/2$, it signifies that the ith entrant has poor fitness and needs to search elsewhere. f_g and f_w are the current best fitness and worst fitness, respectively. When $f_i > f_g$ it suggests that the sparrow is at the edge of the group and vulnerable to predators. If $f_i = f_g$, this means that the individuals in the center of the group are aware of the danger and need to fly to other individuals to reduce the capture risk.

The SSA algorithm has some shortcomings, such as being easy to fall into the local optimal solution and low accuracy. In the initialization phase of SSA, the algorithm generates solutions randomly, and elite sparrows with higher energy storage begin to guide other sparrows in the population to find food. When elite sparrows fall into the local optimization, the foraging rate of all sparrows may slow down or even stagnate, eventually leading to the local optimization of the entire sparrow population. EOBL can search original initial solution and newly generated inverse solution in both directions to give momentum to the elite particles in the population (Tizhoosh, 2005). It can help elite particles jump out of the local extrema and guide

other particles to fly towards the global optimal solution. Tubishat et al. (Tubishat et al., 2019) employed EOBL to improve the population diversity in the initial stage of the whale optimization algorithm (WOA). The EOBL technology was utilized to enhance the quality and speed of solutions of the cuckoo search (CS) algorithm (Huang et al., 2016). Zhang et al. (Zhang et al., 2017) applied the EOBL strategy to avoid the immature convergence of the GWO algorithm by balancing development and exploration. In this paper, the EOBL is adopted for performing the search process simultaneously in all directions and opposite directions of SSA. The mathematical definition is described as follows:

$$X^*_{i,j}(t) = k\left(a_j(t) + b_j(t)\right) - X_{i,j}(t) \quad \text{(Equation 16)}$$

$$a_j(t) = \min\left(X_j(t)\right) \quad \text{(Equation 17)}$$

$$b_j(t) = \max\left(X_j(t)\right) \quad \text{(Equation 18)}$$

$$X^*_{i,j} = rand\left(a_j, b_j\right), \ \ if \ \ X^*_{i,j} < a_j \ or \ X^*_{i,j} > b_j \quad \text{(Equation 19)}$$

where $X_{i,j}(t)$ and $X^*_{i,j}(t)$ represent the current and opposition-based solutions of the *ith* elite sparrow in the *j* dimension, respectively; *t* is the current number of iterations; *k* is a random number between 0 and 1. a_j and b_j correspond to the upper and lower bounders of *jth* decision variable, respectively. The dynamic bounder of the search space replaces the fixed bounder, which is advantageous for preserving the optimal solution. Equation (19) shows that the inverse solution jumps out of the dynamic boundary, which is a feasible solution.

In addition, in the later iteration of SSA, sparrows gradually fly closer to the optimal individual, which easily leads to the loss of population diversity. If the current optimal individual is a locally optimal solution, then the algorithm is easy to fall into the local optimum, especially when solving high-dimensional multimodal functions. Therefore, it should be considered to improve the search speed of the optimal solution to avoid sparrows being attacked by predators. To solve this problem, the Cauchy–Gaussian mutation strategy is added to SSA (Li et al., 2017). Its basic principle is to perform Cauchy–Gaussian mutation operation at the optimal solution position to obtain a new solution. Then, the position before and after mutation is compared, and the better position is selected to execute the next iteration. The mathematical formula is described as follows:

$$M^{t+1}_{\text{best}} = X^t_{\text{best}} \cdot \left[1 + \frac{1 - t^2}{t^2_{\max}} c\left(0, \sigma^2\right) + \frac{t^2}{t^2_{\max}} g\left(0, \sigma^2\right)\right] \quad \text{(Equation 20)}$$

$$\sigma = \begin{cases} 1 & if \ f(X_{\text{best}}) < f(X_i) \\ \exp\left(\dfrac{f(X_{\text{best}}) - f(X_i)}{|f(X_{\text{best}})|}\right) & \text{otherwise} \end{cases} \quad \text{(Equation 21)}$$

where X^t_{best} and M^{t+1}_{best} denote the location of the optimal sparrow before and after mutation, respectively; σ^2 is the standard deviation of the Cauchy–Gaussian mutation operator; *c* and *g* represent random variables satisfying Cauchy distribution and Gaussian distribution, respectively. t_{max} is the maximum number of iterations. In Equation (20), with the increase of *t*, the algorithm can adaptively adjust the dynamic parameters, which is conducive to searching for the approximate optimal solution.

Proposed methodology

For each iteration, the ISSA uses EOBL and the Cauchy–Gaussian mutation strategy to enhance the search speed of the space and to improve the quality of the optimum sparrow. More importantly, during DELM training process, ISSA can reduce the error between the actual value and the predicted value of the network iteration. The implementation flowchart of the SOH estimation algorithm using ISSA-DELM is shown in Figure S2. The algorithm is typically divided into the following six steps:

Step 1. Normalize data: obtain the RW discharge data (voltage and current) and RW charging data (current) of sensors, and calculate two IHIs through Equations (3)–(5). Then normalize these data and divide them into the training set and testing set.

Step 2. Initialize parameter: where W and B represent the weight and bias of DELM respectively. n is the population size, t denotes iteration times, ST represents the safety value of sparrow population, lb and ub are an upper bounder of scaling factor and lower bounder of scaling factor, respectively.

Step 3. SSA for a position update: according to Equations (11)–(15), update the location of producers, entrants, and scouters. If the new position f is smaller than that of the previous position, update the position.

Step 4. EOBL for a position update: According to the size of f, sparrows are ranked from the best to the worst. Note that the smaller f is, the better the sparrow is. The top 30% of sparrows are regarded as elite sparrows, and their positions are updated according to Equations (16)–(19). According to the agreed criterion, sparrows replace the food source with a new location to ensure that the whole evolution process would not recede. The greedy selection is expressed as follows.

$$\begin{cases} X_{i,j}(t+1) = X_{i,j}(t), f\left(X_{i,j}(t)\right) < f\left(X^*_{i,j}(t)\right) \\ X_{i,j}(t+1) = X^*_{i,j}(t), f\left(X_{i,j}(t)\right) \geq f\left(X^*_{i,j}(t)\right) \end{cases} \quad \text{(Equation 22)}$$

where $f(X_{i,j}(t))$ represents the fitness value of the ith sparrow of the t generation in the j dimension, $X_{i,j}(t)$ and $X^*_{i,j}(t)$ are the positions before and after the update, respectively.

Step 5. The Cauchy–Gaussian mutation strategy for updating the best sparrow's position: a new solution is obtained by Cauchy–Gaussian perturbation mutation at the potential optimal solution position according to Equations (20) and (21). And then a greedy selection operator is used to determine whether to replace the original position.

$$\begin{cases} X^{t+1}_{\text{best}} = X^t_{\text{best}}, f\left(X^t_{\text{best}}\right) < f\left(M^t_{\text{best}}\right) \\ X^{t+1}_{\text{best}} = M^t_{\text{best}}, f\left(X^t_{\text{best}}\right) \geq f\left(M^t_{\text{best}}\right) \end{cases} \quad \text{(Equation 23)}$$

Step 6. Terminate: when meeting the termination condition, the optimal parameter combination (W, B) is output as the input of the DELM model, and SOH is obtained through regression. Otherwise, increase the number of iterations by 1 and return to Step 3.

By monitoring the charge and discharge of the battery in real-time, the online voltage and current of the battery can be easily obtained using sensors. Then, two IHIs can be extracted from the battery discharging data. Finally, these IHIs are reprocessed and input into the ISSA-DELM model to realize the online prediction of SOH.

Before the beginning of all experiments, the data of all RW experiments are preprocessed to extract the corresponding health indicators and the battery capacity. In addition, to quantitatively evaluate the performance of the proposed ISSA-DELM algorithm for SOH estimation, the root mean square error (RMSE), mean absolute error (MAE), and the absolute error (AE) are used as evaluation criteria, that is

$$RMSE = \sqrt{\frac{1}{n}\sum (y_i - \hat{y}_i)^2} \quad \text{(Equation 24)}$$

$$MAE = \frac{1}{n}\sum_{i=1}^{n} |\hat{y}_i - y_i| \quad \text{(Equation 25)}$$

$$AE = |\hat{y}_i - y_i| \quad \text{(Equation 26)}$$

where n is the number of samples, y_i and $\hat{y}_i$ refer to the actual SOH and the predicted SOH, respectively.